© 2014. Published by The Company of Biologists Ltd | Development (2014) 141, 3033-3039 doi:10.1242/dev.109041

RESEARCH ARTICLE

The origin and loss of periodic patterning in the turtle shell

Jacqueline E. Moustakas-Verho[1,*], Roland Zimm[1], Judith Cebra-Thomas[2], Netta K. Lempiäinen[1], Aki Kallonen[3], Katherine L. Mitchell[4], Keijo Hämäläinen[3], Isaac Salazar-Ciudad[1,5], Jukka Jernvall[1] and Scott F. Gilbert[1,4,*]

ABSTRACT

The origin of the turtle shell over 200 million years ago greatly modified the amniote body plan, and the morphological plasticity of the shell has promoted the adaptive radiation of turtles. The shell, comprising a dorsal carapace and a ventral plastron, is a layered structure formed by basal endochondral axial skeletal elements (ribs, vertebrae) and plates of bone, which are overlain by keratinous ectodermal scutes. Studies of turtle development have mostly focused on the bones of the shell; however, the genetic regulation of the epidermal scutes has not been investigated. Here, we show that scutes develop from an array of patterned placodes and that these placodes are absent from a soft-shelled turtle in which scutes were lost secondarily. Experimentally inhibiting Shh, Bmp or Fgf signaling results in the disruption of the placodal pattern. Finally, a computational model is used to show how two coupled reaction-diffusion systems reproduce both natural and abnormal variation in turtle scutes. Taken together, these placodal signaling centers are likely to represent developmental modules that are responsible for the evolution of scutes in turtles, and the regulation of these centers has allowed for the diversification of the turtle shell.

KEY WORDS: Shh, Ectodermal appendage, Placode, Scute, Turtle

INTRODUCTION

Recent studies of turtle development and paleontology (Cebra-Thomas et al., 2005; Nagashima et al., 2007; Li et al., 2008; Moustakas, 2008; Sánchez-Villagra et al., 2009; Kawashima-Ohya et al., 2011; Kuratani et al., 2011; Hirasawa et al., 2013) have advanced our understanding of the evolutionary origin of turtles and the genetic and cellular interactions that regulate various aspects of bone development in the carapace. However, the genetic regulation of the origin and evolution of the epidermal scutes has not been addressed. Scutes are plate-like keratinous cutaneous appendages that grow radially and contiguously in the epidermis (Alibardi, 2006), and their presence is a basal trait in extant turtles, as they were present at least 210 million years ago in *Proganochelys* (Gaffney, 1990). Their tessellation and pigmentation are diagnostic to the species level, although they have been lost or reduced in certain freshwater (trionychid, *Natator*) and marine (*Dermochelys*) taxa. The epidermal layer of the hard-shelled slider turtle *Trachemys scripta* generally consists of 38 scutes in the carapace and 16 in the plastron. The bones of the turtle shell form later in development than the scutes and have a pattern different from that of the scutes (Zangerl, 1969).

Turtle scutes, like feathers, are generally thought to have been derived from the reptilian scale (Maderson, 1972). Feathers, scales, teeth, hair and many exocrine glands develop as ectodermal appendages through epithelial-mesenchymal interaction. Consequently, turtle scutes have been proposed to develop from local epithelial thickenings called placodes (Cherepanov, 2006), although this remains to be demonstrated. Unlike scales, feathers and hair, turtle scutes grow radially within the plane of the epidermis. Turtle scutes, therefore, form modules that maintain their growth in apposition to one another and coordinate this growth with that of the underlying carapacial and plastral bones (Zangerl, 1969; Alibardi, 2005). To address the developmental origin and regulation of turtle scutes, we examined genes involved in their formation and used this information to construct a computational model to account for the dynamics of scute patterning.

RESULTS

Scutes develop from an array of patterned placodes

The first morphological indication of turtle shell development is the formation of the carapacial ridge at stage Yntema 14 (Y14) (Yntema, 1968). In *T. scripta*, our *in situ* analysis of the expression of bone morphogenetic protein 2 (*Bmp2*), sonic hedgehog (*Shh*), *Bmp4* and the Bmp target gene *Msx2* at stage Y16 showed the appearance of segmented domains along the carapacial ridge, as well as punctate domains of expression dorsally on the developing carapace and ventrally on the developing plastron (Fig. 1A; supplementary material Fig. S1). These domains coincided with thickenings of placodal ectoderm at sites of carapacial and plastral scute formation. The expression of the Bmp antagonist *Gremlin* appeared to be the negative image of these domains, forming the outline of the developing scutes (Fig. 1A). Detailed examination of gene expression patterns in histological sections showed that *Bmp2*, *Bmp4*, *Shh* and *Msx2* were expressed opposite the ribs in an overlapping pattern along the carapacial ridge (Fig. 1A; supplementary material Fig. S1). *Shh* was expressed more anteriorly in each marginal placode, and its expression overlapped with the more medially expressed *Bmp2*. The domain of *Bmp2* expression, in turn, overlapped with the expression domain of *Gremlin*, which was seen posterior to the ribs and opposite the anterior myotomes (Fig. 1A). To confirm that our interpretations were not affected by variation among individual specimens, we examined the expression of *Shh*, *Bmp2* and *Gremlin* on alternating sections of the placodes of the same individual followed by a three-dimensional (3D) analysis of the expression patterns. The results showed an overlapping chain of *Shh-Bmp2-Gremlin* expression (Fig. 1B), suggesting that at the level of molecular signaling, the separate scute primordia are already in apposition to each other.

Scute placodes contour the carapacial ridge

To further examine the structure of scute placodes, we performed a soft tissue X-ray micro-computed tomography analysis of developing

[1]Developmental Biology Program, Institute of Biotechnology, University of Helsinki, P.O. Box 56, Helsinki FIN-00014, Finland. [2]Biology Department, Millersville University, P.O. Box 1002, Millersville, PA 17551, USA. [3]Division of Materials Physics, Department of Physics, University of Helsinki, P.O. Box 64, Helsinki FIN-00014, Finland. [4]Biology Department, Swarthmore College, 500 College Avenue, Swarthmore, PA 19081, USA. [5]Departament de Genètica i Microbiologia, Universitat Autònoma de Barcelona, 08193 Cerdanyola del Vallès, Barcelona, Spain.

*Authors for correspondence (jacqueline.moustakas@helsinki.fi; sgilber1@swarthmore.edu)

Received 15 February 2014; Accepted 23 May 2014

Development (2014) 141, 3033-3039 doi:10.1242/dev.109041

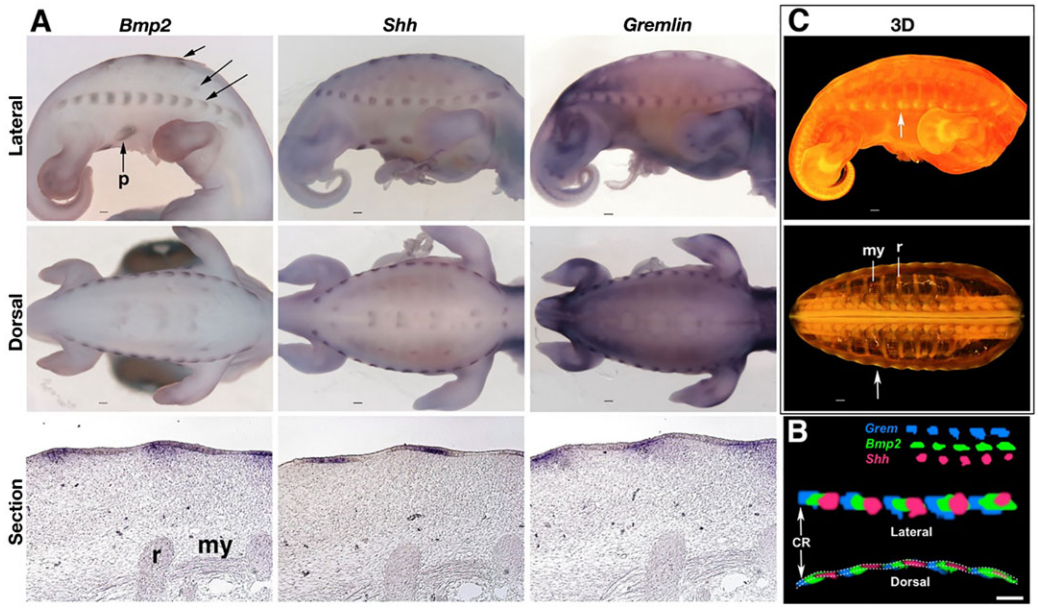

Fig. 1. Expression of *Bmp2*, *Shh* and *Gremlin* viewed laterally, dorsally, and in section in stage Y16 *T. scripta* embryos. (A) *Bmp2* and *Shh* have overlapping expression patterns in the placodal regions (black arrows) that will form the scutes of the turtle shell, whereas *Gremlin* expression appears as the negative image of these domains. (B) 3D reconstruction of developing scutes along the carapacial ridge (CR) from alternate serial sections of the same individual placodes shows an overlapping chain of *Shh* (red), *Bmp2* (green) and *Gremlin* (blue) expression. (C) 3D reconstruction of this stage from soft tissue X-ray micro-computed tomographs shows higher densities in the placodal epithelium of the developing scutes (white arrow) opposite the myotomes. Anterior is toward the right for specimens. Scale bars: 200 µm. p, plastral scute placode; r, rib; my, myotome.

turtles that enables the visualization of tissue condensations (Metscher, 2009). Marginal scute placodes showed the greatest density differences, or contrast, in the epithelium opposite the myotomes (Fig. 1C). Although the carapacial ridge has traditionally been described as a columnar epithelium overlying a condensed mesenchyme (Burke, 1989), we found a periodicity whereby only the epithelium opposite the myotomes is columnar after scute development has begun (supplementary material Movie 1).

Evolutionary and experimental loss of scutes

The importance of these placodal signaling centers for scute development can be tested by studying turtles in which scutes are absent naturally. The aquatic Chinese soft-shelled turtle *Pelodiscus sinensis* does not have keratinized scutes and instead forms a leathery skin. We examined *Pelodiscus* embryos at stages Tokita-Kuratani 15 and 16 (TK15-16) (Tokita and Kuratani, 2001) for their gene expression patterns and scute placodes. These stages are comparable to the same stages of *T. scripta* embryos that we examined above. The results showed that *Pelodiscus* embryos lack the punctate expression of *Shh*, *Bmp2*, *Bmp4*, *Gremlin* and *Msx2* that was seen dorsally and marginally in the hard-shelled turtle *T. scripta*. Instead, these genes in *Pelodiscus* were expressed in a thin line around the carapacial ridge, delineating the perimeter of the developing carapace (Fig. 2A-C; supplementary material Fig. S2). Moreover, the carapacial ridge margin remained unscalloped and scute formation was not initiated.

We next tested experimentally whether disruption of these signaling pathways would affect the patterning of scutes. In cultured *T. scripta* embryos that had been treated with an inhibitor of hedgehog (Hh) signaling [cyclopamine (cyc)] (Chen et al., 2002) or an inhibitor of Bmp signaling (LDN193189) (Cuny et al., 2008), the segmented pattern of *Shh* expression was lost from the carapace (Fig. 2D-F), indicating that these pathways interact during the formation of the turtle scutes. Both Shh and Bmp signaling, therefore, are necessary for the expression of *Shh* in the scute placode. Like the embryos of *Pelodiscus*, the carapacial ridges of these embryos do not have a contoured outline, which is characteristic of scute development, but rather the carapacial ridge is uniform in structure along its length (Fig. 2E,F). In control embryos, scute placodes were seen as protrusions of the carapacial ridge and were marked by *Shh* expression (Fig. 2D).

We next examined the potential roles of fibroblast growth factor (Fgf) signaling in turtle scute development by culturing *T. scripta* embryos with an inhibitor of FGF receptor (SU5402) (Mandler and Neubüser, 2001; Mohammadi et al., 1997). In these cultures, the regular distribution of marginal *Shh* expression was severely disrupted (Fig. 2G,H), effectively randomizing the placodal patterns (Runs test: P=0.17-1, except for the left sides of samples 1 and 10, P=0.04 and P=0.02, respectively, Fig. 2I).

Dynamics of developing carapacial scutes

Trachemys scripta, like most hard-shelled turtles, has 38 carapacial scutes that are grouped into 24 marginal, eight costal, five vertebral and one nuchal scutes (Fig. 3A). We examined the developmental sequence of these scutes from placode initiation to the generation of the final scute pattern of the turtle carapace by using *Bmp2* expression. In the formation of each individual scute, we detected an initial domain of expression that progressively expanded radially, resembling a traveling wave that expanded until it encountered the expression domains of the other scutes. In the development of the marginal scutes, we observed the simultaneous appearance of segmented domains along the carapacial ridge at stage Y14-15 (Fig. 3A). These domains are the thickened placodal epithelium of the future marginal scutes. In the area forming costal scutes, *Bmp2* expression was punctate, initially (Y14-15) in four paired domains corresponding to each scute, and these domains expanded until stage Y19. The vertebral scutes began as paired primordia with punctate *Bmp2* expression at Y15 along the dorsal midline, with the fifth pair

Development (2014) 141, 3033-3039 doi:10.1242/dev.109041

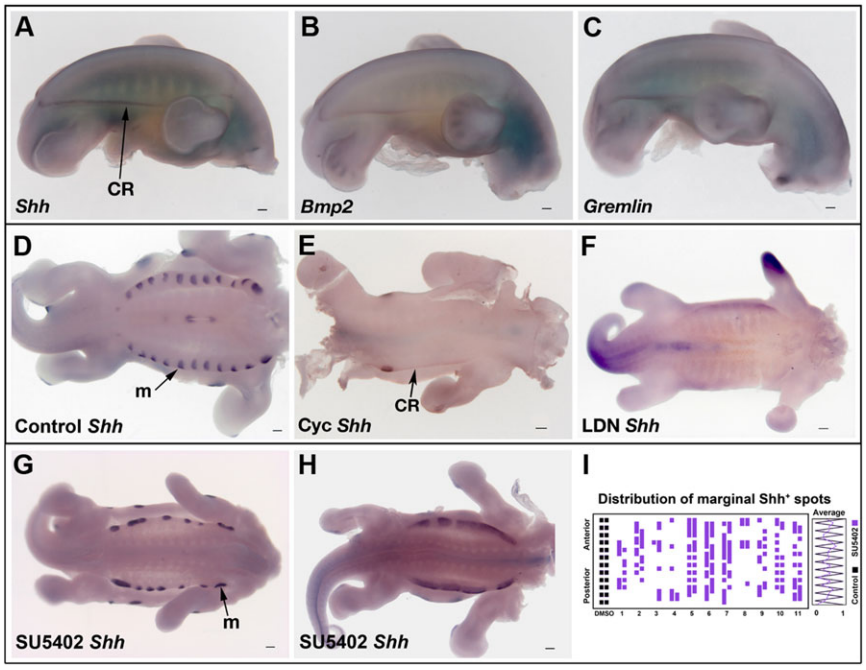

Fig. 2. Evolutionary and experimental loss of turtle scutes and signaling centers. Scuteless *Pelodiscus* embryos lack the punctate expression of *Shh* (A), *Bmp2* (B) and *Gremlin* (C), which are expressed in a line along the expanding carapacial ridge. No serrations are seen at the borders of the carapacial ridge (CR). (D-F) Experimental loss of the placodal signaling centers. A control cultured *T. scripta* embryo (D) shows *Shh* expression in the scute placodes along the carapacial ridge (arrows), whereas embryos cultured with the Shh signaling inhibitor cyclopamine (Cyc) (E) and the Bmp signaling inhibitor LDN193189 (LDN) (F) lose *Shh* expression in these regions. (G-I) Fgf signaling is necessary for scute patterning. (G,H) *T. scripta* embryos cultured with SU5402 show fusions and absences of domains expressing *Shh* along the carapacial ridge. (I) A graphical representation of these samples reveals that the distribution of marginal *Shh* expression shows a great degree of variation in treated turtles compared with the controls (treated with dimethylsulfoxide). Only the left sides of samples 1 and 10 depart from randomness in the SU5402-treated turtles (Runs test). Anterior is toward the right for specimens and toward the top in the graph. Scale bars: 200 µm. m, marginal scute primordia.

of vertebral scute primordia being the last to form posteriorly by Y17. The paired vertebral scute primordia began to merge together around stage Y17. The nuchal scute also developed as a pair of primordia at Y16 and fused at later stages. By Y20, each of the carapacial scute primordia had grown radially and was in apposition to its neighboring scutes (Fig. 3A). The regions between scutes, called seams, can leave a depression (sulcus) on the underlying dermal bones.

A computational model of scute formation and variation

The sequence of scute induction and growth are suggestive of a system that is patterned by Turing mechanisms. Reaction-diffusion dynamics have been hypothesized to be responsible for the patterning of ectodermal appendages, such as hair and feathers (Sick et al., 2006; Painter et al., 2012; Chuong et al., 2013). In those systems, a diffusible extracellular activator signal promotes its own synthesis and the synthesis of an inhibitory extracellular diffusible signal that represses activator synthesis. As a result, a symmetry break occurs and an ordered spatial pattern of homogeneously spaced spots or stripes arises (Koch and Meinhardt, 1994; Kondo and Miura, 2010). To explore whether similar dynamics could account for placodes giving rise to turtle scutes, we constructed a mathematical model of scute formation from an initial set of placodes. The model includes two reaction-diffusion systems, one for the positioning of the initial expression domain of each scute and one for the traveling wave expansion of these expression domains, coupled with growth. Each reaction-diffusion system is based on the basic Meinhardt–Gierer model (Gierer and Meinhardt, 1972). Our model starts from an initial condition in which the first activator (A_1; t=0) is expressed in 12 spots in the margins (Fig. 3B; supplementary materials and methods). This initial condition follows from the observation of a pre-pattern of 12 marginal scute placodes on each carapacial ridge that we hypothesize to be established by the somites, the segmental units of paraxial mesoderm on either side of the neural tube and notochord in vertebrate embryos (Yntema, 1970; Nagashima et al., 2007; Moustakas, 2008). We identified this pre-pattern with the sequentially alternating expression domains of Gremlin-Shh-Bmp in the carapacial ridge that are shown in Fig. 1B. The first activator-inhibitor couplet in the model results in the formation of the relative positions of the presumptive scute placodes, comprising two columns of 12 marginal, four costal and six vertebral scutes (the paired nuchal scute primordia are induced as vertebrals, resulting in six pairs of 'vertebral' scutes; Fig. 3B). The placodal pattern induces the second reaction-diffusion system, which creates the final scute architecture as a result of activator and inhibitor traveling waves that propagate from the scute signaling centers (Fig. 3B; supplementary material Fig. S3, supplementary materials and methods). The simulations show that the model closely approximates the processes of scute formation in our data (Fig. 3; supplementary material Movie 2A,B), suggesting that the mechanisms underlying turtle scute formation are consistent with the two phases of activator-inhibitor dynamics in a growing domain.

Testing the model on scute patterning

To test experimentally our mathematical model of scute formation, we cultured *Trachemys* embryos at various stages with beads that had been soaked in proteins of potential activators or inhibitors in our system. We found the timing and location of bead placement to be important variables in determining the appearance of a phenotypic response, and variant phenotypes were only observed in cultures where beads were placed, at least, slightly off-center from the midline (Fig. 4; supplementary material Figs S4 and S5). Placing a bead soaked in human recombinant SHH protein on explants before the final array of scute placodes were induced – i.e. during the activity of the first reaction-diffusion system (Y15-16) – induced a clustering of smaller additional spots of *Shh* expression adjacent to the bead (Fig. 4Ai). In the model, we can simulate the ectopic addition of local sources of hypothetical activator, inhibitor or their upstream regulator proteins (supplementary material Fig. S4). We found that placing an ectopic source of a hypothetical inhibitor of the inhibitor of the first reaction-diffusion system mimicked the phenotype seen in our early SHH bead cultures (Fig. 4Aii), suggesting that SHH is an (indirect) activator in the first reaction-diffusion system (Fig. 4A; supplementary material Fig. S4). By contrast, a similarly placed bead soaked in human recombinant FGF4 protein during the activity of the first reaction-diffusion

Development (2014) 141, 3033-3039 doi:10.1242/dev.109041

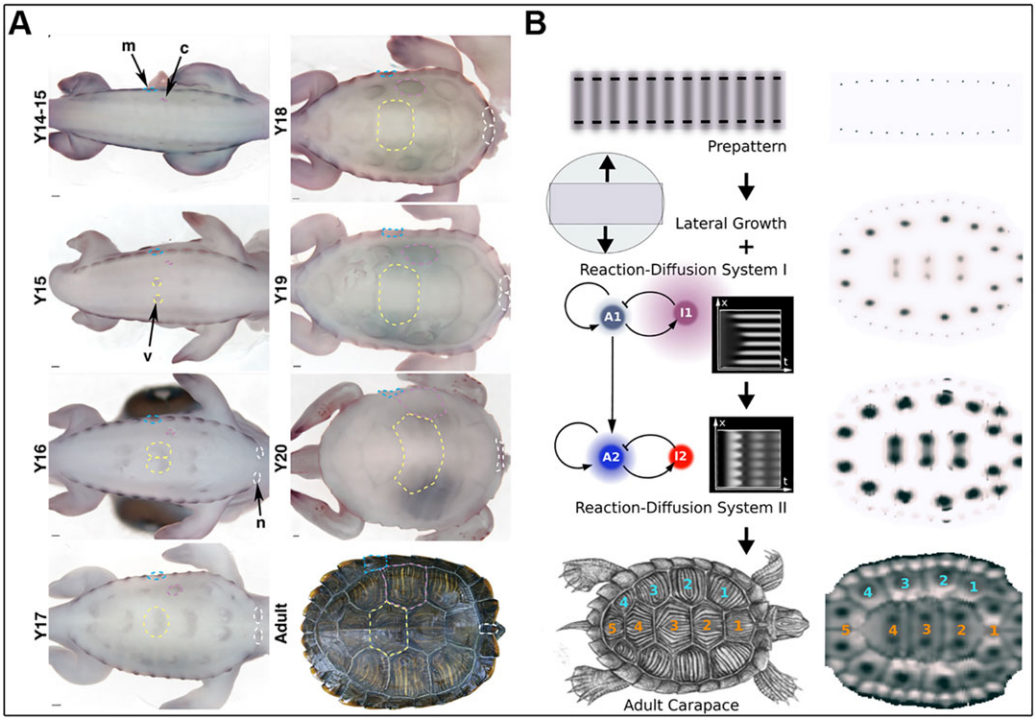

Fig. 3. Dynamics of carapacial scute formation in *T. scripta* visualized using *in situ* hybridization and as a mathematical model. (A) Following the formation of the carapacial ridge, by using *in situ* hybridization, we observed that *Bmp2* is expressed segmentally in the developing marginal (m, blue outline) scutes; expression is also seen in the costal (c, pink outline) scute primordia. Around Y15, expression is seen in the paired vertebral (v, yellow outline) scute primordia. At stage Y16, expression is seen in the paired nuchal (n, white outline) scute primordia. At later stages, *Bmp2* expression is seen at the anterior margins of the developing scutes. Expression is also seen in the developing scales of the limbs and tail (Y20). Fully differentiated keratinized *T. scripta* scutes are seen in the adult specimen (photo credit of adult specimen: Bob Smither). Anterior is toward the right. For illustrative purposes, dashed outlines followed scute primordia through the stages. Scale bars: 200 µm. (B) Hypothesis of scute pattern formation and dynamics of its implementation in a mathematical model. From a pre-pattern of 24 marginal spots, as set by the somites, a first reaction diffusion system (A_1, activator; I_1, inhibitor) is induced, whose steady state is a stable Turing pattern of 38 spots. The small *x*-*y* plot insert depicts the spatio-temporal dynamics of Turing pattern formation (*x*-axis, time; *y*-axis, position; white, concentration of activator; arbitrary units). This pattern induces a second reaction-diffusion system with different parameters (A_2, activator; I_2, inhibitor). In addition, we include lateral outgrowth of the carapace, which is seen to occur concomitantly. This is represented by a gray square growing progressively to an ellipsoid, as the arrows indicate. Finally, the second reaction-diffusion system produces the outlines of the 38 adult carapacial scutes by a spatiotemporally unstable traveling-wave mechanism (dynamics shown as *x*-*y* time-space plot insert). The seams between the scutes are suggested to form where traveling waves of A_2 or I_2 collide. On the right side, activator concentrations in model simulations are plotted for A_1,t=0; A_1,t=230,000; A_2,t=236,000; A_2,t=240,000 (from top to bottom). The final scute architecture is generated by traveling waves, resulting in 24 marginal, eight costal and six vertebral (five vertebral plus one nuchal) scutes, as seen in *T. scripta*. Vertebral scutes are numbered in orange, costal scutes in blue. *T. scripta* adult carapace illustration by Tiff Shao.

system results in the local absence of *Shh* expression (Fig. 4Aiii). Combining this result with our model simulations, we hypothesize that FGF4 is acting as an inhibitor (or the activator of an inhibitor) in the first reaction-diffusion system (Fig. 4Aiv). These experiments and simulations, therefore, suggest that Shh and Fgf signaling act in the first reaction-diffusion system of the model that normally produces a regularly patterned array of 38 scute placodes. Placing a bead soaked in SHH protein later in development, during the activity of the second reaction-diffusion system (Y17), results in the production of a supernumerary scute adjacent to or underneath the bead (Fig. 4B). The induction of a supernumerary scute, combined with simulation data (Fig. 4B; supplementary material Figs S4 and S5), suggests that SHH is acting as an activator in the second reaction-diffusion system.

Many turtles show anomalous intra-species variation, including supernumerary and fused scutes (Coker, 1910; Yntema, 1970). Some of our embryos show anomalous patterns in the distribution of scute primordia (as shown by *Bmp2* expression; Fig. 4C), corresponding to the documented adult patterns, including supernumerary misplaced scutes and a zigzag pattern of unfused vertebral scutes (Fig. 4C). To explore whether these phenotypic anomalies could also be produced by our model, we performed a variational analysis by systematically changing the model parameters and comparing the resulting phenotypes. These parameters were changed independently in each of the reaction-diffusion systems because they involve different or differently regulated signals (supplementary material Fig. S6, supplementary materials and methods). All changes in the parameters of the reaction-diffusion system in the model resulted in changes that were symmetrical with respect to the right and left halves of the carapace, and, therefore, did not produce asymmetric scute patterns, which were seen in intra-specific variants. Furthermore, adding moderate gene expression noise did not reproduce these variants; such noise only slightly blurred the spots that formed by reaction-diffusion dynamics but did not randomize their positions. Morphological patterns resembling naturally occurring anomalies arose in the model, however, by hemispheric offsets in the marginal placodes or growth asymmetry (Fig. 4C; supplementary material Figs S7 and S8).

Finally, most hard-shelled turtles have the same number of carapacial scutes as *T. scripta*. Loggerhead (*Caretta caretta*) and ridley sea turtles (*Lepidochelys olivacea* and *Lepidochelys kempii*), however, have five and six to seven pairs of costal scutes, respectively, and show a greater range of variation in scute numbers naturally (Bull and Vogt, 1979; Mast and Carr, 1989). These species vary in their

Development (2014) 141, 3033-3039 doi:10.1242/dev.109041

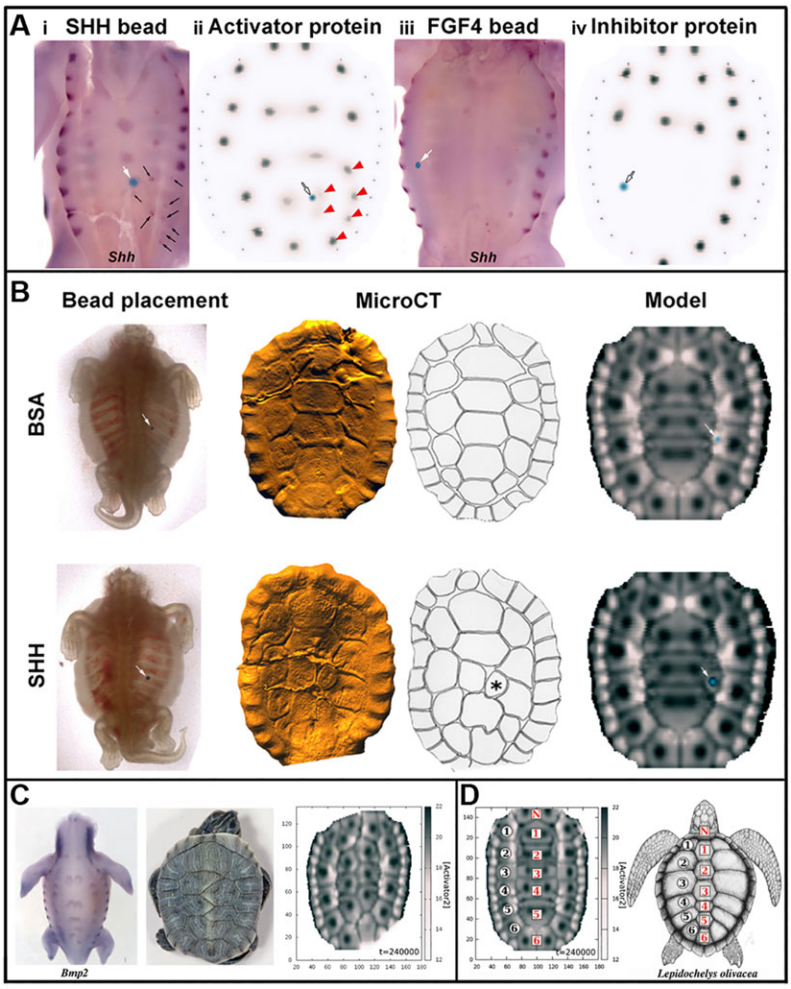

Fig. 4. Testing the model on scute patterning. (A,B) The role of proteins in scute pattern formation can be tested by implanting protein-coated beads as an additional source of diffusible protein both *in vitro* and *in silico*. (A) Early (Y15-16) implantation of a SHH-coated bead (Ai) causes a number of small and narrowly spaced *Shh* spots (black arrows) to arise adjacent to the bead after culture, as visualized by *in situ* hybridization. A similar pattern is produced by the ectopic addition of an inhibitor of I_1 (i.e. an indirect activator) in the model (Aii; A_1, t=210,000; red arrowheads). By contrast, implantation of an FGF4-coated bead (Aiii) results in a large field with no *Shh* spot formation. In the model, the addition of a source of activator of I_1 (i.e. an inhibitor) prevents spot formation in an area around the bead, the size of which depends on the concentration and the diffusion rate used (Aiv; A_1, t=210,000). (B) Late (Y17) implantations of a SHH-coated bead results in the formation of a supernumerary scute, compared with the addition of a bovine serum albumin-coated (control) bead. The cultures (left) show bead placement at the time of implantation, and the resulting cultures were analyzed using micro-computed tomography (MicroCT) scans (center panel shows 3D scan and line drawing). The results of model simulations (A_2, t=240,000) for control and bead experiments with an additional source of I_2 (i.e. an inhibitor are illustrated) (right). The locations of beads on cultures and ectopic sources of protein in simulations are shown by white arrows. (C,D) Mathematical models of abnormal and natural variation in turtle scute patterns. (C) Scute variation occurs spontaneously in natural populations of turtles (left). Similar variation in scute patterns is also observed occasionally in embryonic specimens (revealed by *Bmp2* expression, middle). This anomalous variation can be produced by the introduction of a hemispheric offset into the model (right). (D) Elongating the initial anterior-posterior axis in the model produces additional costal and sometimes vertebral scutes, as seen in *L. olivacea*. Anterior is towards the top. Vertebral scutes are numbered in red, costal scutes in black. N, nuchal. Time is given in simulation steps. *L. olivacea* illustration by Tiff Shao.

numbers of marginal scutes, and *Lepidochelys* often have a greater number of vertebral scutes (Fig. 4D). Our computational model was able to reproduce variation that was consistent with this interspecific variation. The most parsimonious way to change the number of scutes symmetrically is by changing the length of the anterior-posterior axis, either by increasing or decreasing the longitudinal carapacial area; as a consequence, the number of costal and vertebral scutes became modified (Fig. 4D; supplementary material Fig. S9).

DISCUSSION

In this study we provide evidence that the scutes of the turtle shell originate from the formation of a patterned array of signaling modules on the carapace and plastron, and that this set of developmental modules was modified in the evolution of turtle scutes to accommodate their planar growth.

Although ectodermal appendages are very different morphologically, the early steps of their morphogenesis are regulated by several relatively well-characterized signaling pathways including the transforming growth factor β (Tgfβ), Hh, Fgf and Wnt families, and their downstream transcription factors (Pispa and Thesleff, 2003). First we examined ectodermal placodal markers *Bmp2*, *Bmp4*, the Bmp target gene *Msx2*, the Bmp antagonist *Gremlin* and *Shh* in turtle embryos because research on birds and alligators has implicated Bmp and Shh signaling in regulating feather and scale development at various stages (Nohno et al., 1995; Noramly and Morgan, 1998; Harris et al., 2002; Bardot et al., 2004). Previously, we had found several of these genes to be expressed in the developing dermatomes of *T. scripta*; however, their role in scute development was not investigated (Moustakas, 2008). Our results showing the expression of these genes in developing turtle scutes reveal that scute placodes express the same sets of genes as the placodes for alligator scales and avian scales and feathers, in which there are adjacent expression domains of *Bmp2* anteriorly and *Shh* posteriorly in each placode (Harris et al., 2002). However, in scales and feathers, these domains are separate, whereas in the scutes, they partially overlap.

Furthermore, unlike the development of feathers, hair and teeth, where the mesenchyme forms a pronounced dermal condensate directly under the thickened epithelium, the mesenchyme of the developing scutes appears to be condensed uniformly along the carapacial ridge (Fig. 1A).

Our experimental data demonstrate that Shh and Bmp signaling are necessary for the formation of the scutes of the turtle shell and that Fgf signaling is necessary for the segmented distribution of *Shh* expression in the marginal scute placodes (Fig. 2). These results are in agreement with the proposed integration of the Shh- and Bmp-mediated signaling pathways in the morphogenesis (Nohno et al., 1995; Noramly and Morgan, 1998; Harris et al., 2002) and spacing (Noramly and Morgan, 1998; Bardot et al., 2004) of the placodes during feather and scale development. Similarly, Fgf signaling has been implicated in the patterning of feathers (Mandler and Neubüser, 2004; Song et al., 2004; Wells et al., 2012), and we have previously shown *Fgf8* and *Fgf10* to be expressed in the developing carapace of *T. scripta* (Loredo et al., 2001; Cebra-Thomas et al., 2005).

Development (2014) 141, 3033-3039 doi:10.1242/dev.109041

We hypothesize that the loss of the placodes led to the evolutionary loss of the epidermal scutes in soft-shelled turtles, an adaptation that permits dermal breathing and adaptive muscular control of the shape of the shell in such soft-shelled turtles (Dunson, 1960; Wang et al., 1989). We note that the expression patterns along the carapacial ridge of *Pelodiscus* resemble that of *Gremlin* in *T. scripta* before scute development is initiated (Moustakas, 2008), suggesting that scute development in *Pelodiscus* is arrested before patterned expression of *Shh* and *Bmp* genes.

The positioning of placodes and their posterior expansion is consistent with a two-phase reaction-diffusion system with growth (Fig. 3), and our hypotheses implicating Shh signaling in the reaction-diffusion dynamics of turtle scute formation are consistent with the patterning of other vertebrate organ systems, such as the teeth, palatal rugae and limbs (Cho et al., 2011; Economou et al., 2012; Sheth et al., 2012). Reaction-diffusion systems have also been proposed to play a role in the development of other ectodermal appendages. However, unlike feathers and hair, which have adopted a proximal-distal mode of growth from an ancestral scale (Maderson, 1972), turtle scutes grow radially and might require a second reaction-diffusion system to form their final shape of interlocking modules.

Turtle scute patterns show a paradox as being highly conserved between groups of turtles but having a great individual variety within each group of turtles (Zangerl and Johnson, 1957; Zangerl, 1969). Scute anomalies have been attributed to mechanical stresses (Yntema, 1970), such as those produced by desiccation (Coker, 1910), high temperature (Gardner Lynn and Ullrich, 1950) and environmental pollution (Bujes and Verrastro, 2007). Based on the simulation experiments of our computational model (Fig. 4), we hypothesize that these environmental stresses are translated into asymmetric growth in the embryo. Interestingly, because scute anomalies have been documented to occur more often in females (Gardner Lynn and Ullrich, 1950), and because most turtles have temperature-dependent sex determination in which higher temperatures yield females (Van Meter et al., 2006), high temperatures might be a factor disturbing the placodal pre-pattern. Finally, we were also able to reproduce the natural variation seen in marine turtles, which have a wider range in the number of scutes than most hard-shelled turtles.

Taken together, the development, the loss, and the variation within and between species of turtle scutes suggest how evolutionary novelties arise and how they can be modified to produce new variants.

MATERIALS AND METHODS

Embryos and staging

Trachemys scripta elegans eggs were collected from commercial turtle farms in Louisiana, USA. Eggs were incubated in a 1:1 mix of water and vermiculite (w/v) at room temperature. Embryos were fixed in 4% paraformaldehyde (PFA) and dehydrated stepwise into 100% methanol for whole-mount *in situ* hybridization. Embryos used for section *in situ* hybridization were fixed in a formol-alcohol fixative and dehydrated stepwise to 100% ethanol. *Pelodiscus sinensis* embryos fixed in 4% PFA and stored in 100% methanol were kindly provided by Drs Hiroshi Nagashima and Shigeru Kuratani (RIKEN CDB). Embryos were staged as described previously (Tokita and Kuratani, 2001; Yntema, 1968).

In situ hybridization and 3D reconstructions

Probes and the *in situ* hybridization performed were essentially as described by Moustakas (Moustakas, 2008) with the following modifications for the whole-mount *in situ* hybridization: glycine [2 mg/ml in phosphate-buffered saline with Tween (PBST)] was used to stop the Proteinase K reaction; 1% SDS was substituted for 0.1% Tween-20 in the hybridization buffer; following hybridization and RNase A treatment, embryos were washed in 5× SSC/50% formamide/1% SDS six times for 30 minutes each; and embryos were washed in PBST following anti-digoxigenin incubation rather than MABT. For 3D reconstructions of gene expression, alternating sections (10 µm) of the same individual placodes were placed on separate slides followed by *in situ* hybridization. The gene expression was delineated in sections using Pixelmator (http://www.pixelmator.com/) and 3D images were reconstructed using ImageJ 1.43 (http://rsbweb.nih.gov/ij/). Owing to differences in probes, the expression patterns should be considered approximate. For each placode, four to six sections were obtained for each probe.

X-ray micro-computed tomography

Trachemys embryos were fixed with 4% PFA, dehydrated into 70% ethanol and dyed with phosphotungstic acid (#P4006, Sigma), which allows detection of differences in soft tissue densities, for 24 h (Metscher, 2009). The samples were scanned using a custom-built µCT system Nanotom 180 NF (phoenix|x-ray Systems+Services) with a CMOS flat-panel detector (Hamamatsu Photonics) and a high-power transmission-type X-ray nanofocus source with a tungsten anode. The samples were imaged with 80 kV acceleration voltage and 180 µA tube current. Projection images were acquired over a full circle of rotation with 0.3° angular interval, and each projection image was composed of the average of 10 transmission images with a 500 ms exposure time. The measurement geometry resulted in an effective voxel size of 5 µm. The reconstruction from the projection images was performed with reconstruction software datos|x rec supplied by the system manufacturer. The reconstruction was then downsampled to 10 µm voxel resolution and Avizo Fire 6.3 was used to render the 3D image and movie.

In vitro cultures

Explants were prepared and cultured as previously described (Cebra-Thomas et al., 2005). Stage Y15-16 *Trachemys* embryos were dissected free of extraembryonic tissues in HBSS, decapitated, split along the midline and eviscerated. The explants were cultured ventral-side down on Transwell-clear 3 µm nucleopore membranes (Corning-Costar) over DME supplemented with 2% FCS, gentamycin, fungazone and nystatin (Sigma). Control cultures were supplemented with dimethyl sulfoxide (DMSO, Sigma) and hydroxypropylcyclodextrin (HPCD, Sigma).

For inhibition of hedgehog signaling, cyclopamine (C988400, Toronto Research Chemicals) was diluted in 45% w/v hydroxypropylcyclodextrin (HPCD, Sigma) and 10 µg was applied directly to the experimental explants. For inhibition of Bmp signaling, explants were treated with 10 µM LDN-193189 (Stemgent). For inhibition of Fgf signaling, explants were treated with 10 µM SU5402 (SU-GEN).

Protein-coated beads were added to explants (stage Y15-16 or Y17) with forceps to test the effects of ectopic protein sources on the development of scutes. Affi-gel blue beads (Bio-Rad) were washed with PBS and soaked for 1 h at 37°C in recombinant proteins (1 mg/ml SHH; 1 mg/ml BMP2; R&D) or bovine albumin serum (BSA). The same procedure was followed using heparin agarose beads (MCLABs) for recombinant FGF4 protein (1 mg/ml; R&D). The explants were cultured for 5 days at 30°C with 5% CO_2. We used Runs test and Monte Carlo simulations (using PAST, http://folk.uio.no/ohammer/past/index_old.html) to test whether the marginal patterns of *Shh* expression differed from randomness after SU5402 treatments. In these tests, the turtles were assumed to have 23 domains that either were *Shh* positive or negative.

The cultured explants were fixed in 4% PFA, dehydrated in 100% methanol and processed for *in situ* hybridization or X-ray micro-computed tomography. For µCT, the samples were imaged over a full 360° with an angular step of 0.5°, and each projection image was composed of an average of 8500 ms exposures. The measurement geometry resulted in an effective voxel size of 2 µm/vox.

Computational model of turtle scute development

The computational model of turtle scute development (available with the source code at http://dead.cthulhu.fi/turtlem/) implements two coupled reaction-diffusion systems and growth in a two-dimensional epithelium representing the developing carapace. Each reaction-diffusion system includes two diffusible extracellular molecules, the kinetics of which are derived from the classic Meinhardt-Gierer equations (Gierer and Meinhardt, 1972). Gnuplot (http://www.gnuplot.info/) was used to plot the simulation output. Morphospace was explored by varying model parameters. Further details can be found in the supplementary materials and methods.

Acknowledgements
We thank K. Padian, I. Thesleff, J. Wyneken, G. Cherepanov, J. Parham, I. Salvador Martínez, K. MacCord, V. Moustakas and P. Holroyd for discussions; A. Vihera, R. Savolainen, J. Garten, A. Stager, K. Verho, T. Kankaanpää, T. Häkkinen and M. Holopainen for technical assistance; H. Nagashima and S. Kuratani for staged *Pelodiscus sinensis* embryos; Tiff Shao for illustrations; Bob Smither for the photograph of the adult *T. scripta* specimen.

Competing interests
The authors declare no competing financial interests.

Author contributions
J.E.M.-V. and J.C.-T. acquired specimens and performed culture experiments; J.E.M.-V. and N.K.S. performed gene expression studies; A.K., J.E.M.-V. and K.H. designed and performed the micro-computed tomography experiments; R.Z. and I.S.-C. designed the model and R.Z. implemented it; K.M. participated in designing the project; J.E.M.-V., R.Z., I.S.-C., S.F.G. and J.J. designed the project and wrote the paper.

Funding
This study was funded by the Academy of Finland; National Science Foundation [RUI-0748508 and DEB-0408163]; Millersville University; a Development Travelling Fellowship; and The Company of Biologists.

Supplementary material
Supplementary material available online at
http://dev.biologists.org/lookup/suppl/doi:10.1242/dev.109041/-/DC1

References

Alibardi, L. (2005). Proliferation in the epidermis of chelonians and growth of the horny scutes. *J. Morphol.* **265**, 52-69.
Alibardi, L. (2006). Ultrastructural and immunohistochemical observations on the process of horny growth in chelonian shells. *Acta Histochem.* **108**, 149-162.
Bardot, B., Lecoin, L., Fliniaux, I., Huillard, E., Marx, M. and Viallet, J. P. (2004). Drm/Gremlin, a BMP antagonist, defines the interbud region during feather development. *Int. J. Dev. Biol.* **48**, 149-156.
Bujes, C. S. and Verrastro, L. (2007). Supernumerary epidermal shields and carapace variation in Orbigny's slider turtles, *Trachemys dorbigni* (Testudines, Emydidae). *Revista Brasileira de Zoologia* **24**, 666-672.
Bull, J. J. and Vogt, R. C. (1979). Temperature-dependent sex determination in turtles. *Science* **206**, 1186-1188.
Burke, A. C. (1989). Development of the turtle carapace: implications for the evolution of a novel bauplan. *J. Morphol.* **199**, 363-378.
Cebra-Thomas, J., Tan, F., Sistla, S., Estes, E., Bender, G., Kim, C., Riccio, P. and Gilbert, S. F. (2005). How the turtle forms its shell: a paracrine hypothesis of carapace formation. *J. Exp. Zool. B Mol. Dev. Evol.* **304B**, 558-569.
Chen, J. K., Taipale, J., Cooper, M. K. and Beachy, P. A. (2002). Inhibition of Hedgehog signaling by direct binding of cyclopamine to Smoothened. *Genes Dev.* **16**, 2743-2748.
Cherepanov, G. O. (2006). Ontogenesis and evolution of horny parts of the turtle shell. *Fossil Turtle Res.* **1**, 19-33.
Cho, S.-W., Kwak, S., Woolley, T. E., Lee, M.-J., Kim, E.-J., Baker, R. E., Kim, H.-J., Shin, J.-S., Tickle, C., Maini, P. K. et al. (2011). Interactions between Shh, Sostdc1 and Wnt signaling and a new feedback loop for spatial patterning of the teeth. *Development* **138**, 1807-1816.
Chuong, C.-M., Yeh, C.-Y., Jiang, T.-X. and Widelitz, R. (2103). Module-based complexity formation: periodic patterning in feathers and hairs. *Wiley Interdiscip. Rev. Dev. Biol.* **2**, 97-112.
Coker, R. E. (1910). Diversity in the scutes of Chelonia. *J. Morph.* **21**, 1-75.
Cuny, G. D., Yu, P. B., Laha, J. K., Xing, X., Liu, J.-F., Lai, C. S., Deng, D. Y., Sachidanandan, C., Bloch, K. D. and Peterson, R. T. (2008). Structure-activity relationship study of bone morphogenetic protein (BMP) signaling inhibitors. *Bioorg. Med. Chem. Lett.* **18**, 4388-4392.
Dunson, W. A. (1960). Aquatic respiration in Trionyx spinifer asper. *Herpetologica* **16**, 227-283.
Economou, A. D., Ohazama, A., Porntaveetus, T., Sharpe, P. T., Kondo, S., Basson, M. A., Gritli-Linde, A., Cobourne, M. T. and Green, J. B. A. (2012). Periodic stripe formation by a Turing mechanism operating at growth zones in the mammalian palate. *Nat. Genet.* **44**, 348-351.
Gaffney, E. S. (1990). The comparative osteology of the Triassic turtle Proganochelys. *Bull. Amer. Mus. Nat. Hist.* **194**, 1-263.
Gardner Lynn, W. and Ullrich, M. C. (1950). Experimental production of shell abnormalities in turtles. *Copeia* **4**, 253-262.
Gierer, A. and Meinhardt, H. (1972). A theory of biological pattern formation. *Kybernetik* **12**, 30-39.
Harris, M. P., Fallon, J. F. and Prum, R. O. (2002). Shh-Bmp2 signaling module and the evolutionary origin and diversification of feathers. *J. Exp. Zool.* **294**, 160-176.
Hirasawa, T., Nagashima, H. and Kuratani, S. (2013). The endoskeletal origin of the turtle carapace. *Nat. Commun.* **4**, 2107.
Kawashima-Ohya, Y., Narita, Y., Nagashima, H., Usuda, R. and Kuratani, S. (2011). Hepatocyte growth factor is crucial for development of the carapace in turtles. *Evol. Dev.* **13**, 260-268.
Koch, A. J. and Meinhardt, H. (1994). Biological pattern formation: from basic mechanisms to complex structures. *Rev. Mod. Phys.* **66**, 1481-1507.
Kondo, S. and Miura, T. (2010). Reaction-diffusion model as a framework for understanding biological pattern formation. *Science* **329**, 1616-1620.
Kuratani, S., Kuraku, S. and Nagashima, H. (2011). Evolutionary developmental perspective for the origin of turtles: the folding theory for the shell based on the developmental nature of the carapacial ridge. *Evol. Dev.* **13**, 1-14.
Li, C., Wu, X.-C., Rieppel, O., Wang, L.-T. and Zhao, L.-J. (2008). An ancestral turtle from the Late Triassic of southwestern China. *Nature* **456**, 497-501.
Loredo, G. A., Brukman, A., Harris, M. P., Kagle, D., Leclair, E. E., Gutman, R., Denney, E., Henkelman, E., Murray, B. P., Fallon, J. F. et al. (2001). Development of an evolutionarily novel structure: fibroblast growth factor expression in the carapacial ridge of turtle embryos. *J. Exp. Zool.* **291**, 274-281.
Maderson, P. F. A. (1972). On how an archosaurian scale might have given rise to an avian feather. *Amer. Nat.* **106**, 424-428.
Mandler, M. and Neubüser, A. (2001). FGF signaling is necessary for the specification of the odontogenic mesenchyme. *Dev. Biol.* **240**, 548-559.
Mandler, M. and Neubüser, A. (2004). FGF signaling is required for initiation of feather placode development. *Development* **131**, 3333-3343.
Mast, R. B. and Carr, J. L. (1989). Carapacial scute variation in Kemp's ridley sea turtle (*Lepidochelys kempi*) hatchlings and juveniles. In *Proceedings of the First International Symposium on Kemp's Ridley Sea Turtle Biology, Conservation and Management* (ed. C. W. Caillouet, Jr and A. M. Landry), pp. 202-219. Texas: A & M University Sea Grant. TAMU-SG-89-105.
Metscher, B. D. (2009). MicroCT for comparative morphology: simple staining methods allow high-contrast 3D imaging of diverse non-mineralized animal tissues. *BMC Physiol.* **9**, 11.
Mohammadi, M., McMahon, G., Sun, L., Tang, C., Hirth, P., Yeh, B. K., Hubbard, S. R. and Schlessinger, J. (1997). Structures of the tyrosine kinase domain of fibroblast growth factor receptor in complex with inhibitors. *Science* **276**, 955-960.
Moustakas, J. E. (2008). Development of the carapacial ridge: implications for the evolution of genetic networks in turtle shell development. *Evol. Dev.* **10**, 29-36.
Nagashima, H., Kuraku, S., Uchida, K., Ohya, Y. K., Narita, Y. and Kuratani, S. (2007). On the carapacial ridge in turtle embryos: its developmental origin, function and the chelonian body plan. *Development* **134**, 2219-2226.
Nohno, T., Kawakami, Y., Ohuchi, H., Fujiwara, A., Yoshioka, H. and Noji, S. (1995). Involvement of the Sonic hedgehog gene in chick feather formation. *Biochem. Biophys. Res. Commun.* **206**, 33-39.
Noramly, S. and Morgan, B. A. (1998). BMPs mediate lateral inhibition at successive stages in feather tract development. *Development* **125**, 3775-3787.
Painter, K. J., Hunt, G. S., Wells, K. L., Johansson, J. A. and Headon, D. J. (2012). Towards an integrated experimental-theoretical approach for assessing the mechanistic basis of hair and feather morphogenesis. *Interface Focus* **2**, 433-450.
Pispa, J. and Thesleff, I. (2003). Mechanisms of ectodermal organogenesis. *Dev. Biol.* **262**, 195-205.
Sánchez-Villagra, M. R., Müller, H., Sheil, C. A., Scheyer, T. M., Nagashima, H. and Kuratani, S. (2009). Skeletal development in the Chinese soft-shelled turtle *Pelodiscus sinensis* (Testudines: Trionychidae). *J. Morphol.* **270**, 1381-1399.
Sheth, R., Marcon, L., Bastida, M. F., Junco, M., Quintana, L., Dahn, R., Kmita, M., Sharpe, J. and Ros, M. A. (2012). *Hox* genes regulate digit patterning by controlling the wavelength of a Turing-type mechanism. *Science* **338**, 1476-1480.
Sick, S., Reinker, S., Timmer, J. and Schlake, T. (2006). WNT and DKK determine hair follicle spacing through a reaction-diffusion mechanism. *Science* **314**, 1447-1450.
Song, H.-K., Lee, S.-H. and Goetinck, P. F. (2004). FGF-2 signaling is sufficient to induce dermal condensations during feather development. *Dev. Dyn.* **231**, 741-749.
Tokita, M. and Kuratani, S. (2001). Normal embryonic stages of Chinese softshelled turtle *Pelodiscus sinensis* (Trionychidae). *Zool. Sci.* **18**, 705-715.
Van Meter, R. J., Spotila, J. R. and Avery, H. W. (2006). Polycyclic aromatic hydrocarbons affect survival and development of common snapping turtle (*Chelydra serpentina*) embryos and hatchlings. *Environ. Pollut.* **142**, 466-475.
Wang, Z.-X., Sun, N.-Z. and Sheng, W.-F. (1989). Aquatic respiration in soft-shelled turtles, *Trionyx sinensis*. *Comp. Biochem. Physiol.* **92**, 593-598.
Wells, K. L., Hadad, Y., Ben-Avraham, D., Hillel, J., Cahaner, A. and Headon, D. J. (2012). Genome-wide SNP scan of pooled DNA reveals nonsense mutation in FGF20 in the scaleless line of featherless chickens. *BMC Genomics* **13**, 257.
Yntema, C. L. (1968). A series of stages in the embryonic development of *Chelydra serpentina*. *J. Morph.* **125**, 219-251.
Yntema, C. L. (1970). Extirpation experiments on embryonic rudiments of the carapace of *Chelydra serpentina*. *J. Morph.* **132**, 235-243.
Zangerl, R. (1969). The turtle shell. In Biology of the Reptilia *Vol.* 1 (ed. C. Gans), pp. 311-339. New York: Academic Press.
Zangerl, R. and Johnson, R. G. (1957). The nature of shield abnormalities in the turtle shell. *Fieldiana Geol.* **10**, 341-362.

Supplementary Materials and Methods

Computational model of turtle scute development

The computational model is built by using an already known mechanism to build a pattern of regularly spaced gene expression spot domains. Reaction-diffusion systems are also an already known way to produce the expansion of those domains as traveling waves and their merging (Gierer and Meinhardt, 1972).

This model implements two coupled reaction-diffusion systems and growth in a two-dimensional epithelium representing the developing carapace. Each reaction-diffusion system includes two diffusible extracellular molecules. The activator A_1 for the first reaction-diffusion system promotes its own synthesis and that of its diffusible inhibitor I_1. Equally, in the second reaction-diffusion system the activator A_2 promotes its own synthesis and that of its diffusible inhibitor I_2. In addition, A_1 promotes the production of A_2. The inhibitors repress the synthesis of their respective activators. The initial condition from which the simulations start includes two rows of A1 concentration peaks (see Figs 1, 4) at the margins of the carapace. During the first 150000 iterations, the model includes only growth. At the end of that period starts the first reaction-diffusion system, and after 30000 iterations, an acceleration of growth, according to the development of *T. scripta*. 55000 iterations later, the second reaction-diffusion system is initiated.

Reaction-diffusion kinetics:

The reaction-diffusion equations are derived from the classic Meinhardt-Gierer equations (Gierer and Meinhardt, 1972).

(1) $$\frac{\partial A_1}{\partial t} = \frac{r_1 A_1^2}{1 + k_I I_1} - m_1 A_1 + a_r + D_I \nabla^2 A_1$$

(2) $$\frac{\partial I_1}{\partial t} = r_2 A_1^2 - m_2 I_1 + D_2 \nabla^2 I_1$$

(3) $$\frac{\partial A_2}{\partial t} = \frac{s A_1^2 + r_3 A_2^2}{1 + k_2 I_2} - m_3 A_2 + D_3 \nabla^2 A_2$$

(4) $$\frac{\partial I_2}{\partial t} = r_4 A_2^2 - m_4 I_2 + i_r + D_4 \nabla^2 I_2$$

Here, r_1 and r_2 describe the rate of activation by the activator A_1, and r_3 and r_4 activation by A_2. k_1 and k_2 describe the strength of inhibition of A_1 and A_2 production by I_1 and I_2. a_r is a residual activation of A_1, whereas s is the rate of activation of A_2 by A_1. i_r is a residual activation of I_2. m_1, m_2, m_3, and m_4 give decay rates of the gene products A_1, I_1, A_2, and I_2. D_1, D_2, D_3, and D_4 are the diffusion rates of A_1, I_1, A_2, and I_2.

These parameters are such that the first reaction-diffusion system establishes a pattern of spots of expression of A_1 and I_1 and the second produces traveling waves from these spots that collide with each other to form the hexagon-like scute morphologies. The simulations are performed on a growing grid of square cells (at maximal size this grid reaches 1.5±0.2x10² cells). Every cell is adjacent to four neighbors. Boundary conditions are closed (zero flux). Numerical integration is performed by the Euler method with $\delta=10^{-3}$.

Formation of boundaries between scutes by traveling waves:

The second reaction-diffusion system establishes the locations of future scute boundaries. In it concentration peaks of activator (A_2) and inhibitor (I_2) propagate centripetally from the spots of high A_1 expression (cf. Fig. 3), which have been previously positioned as a Turing pattern by the first reaction-diffusion system.

The propagation of these peaks occurs as a traveling wave phenomenon that emerges from the reaction-diffusion system. The same equations are used in the first and second reaction-diffusion systems but in the second reaction-diffusion system, the activator diffuses faster than its inhibitor, i.e. $D_3 > D_4$. Auto-activation of the activator leads to a fast increase in the concentration of activator, and, with a small but important delay, of the inhibitor, which starts repressing the increase of the activator. Since the activator diffuses faster than the inhibitor, the relative increase of activator is highest at the edges of its spatial extension, where activator molecules have just arrived by diffusion but inhibitor has had not time to arrive yet (Fig. S3). Thus, the highest concentration of activator is found in a temporally extending concentric ring around the spots of high expression of A_1. Consequently, an inhibitor wave is seen following the wave of activator concentration (Fig. S3A-B).

The traveling waves expanding from the center of each forming scute end up colliding with each other in space and, as a result, form the stable (non-traveling) boundaries between scutes (Fig. 3). The traveling waves can only spread where there is no inhibitor (since inhibitor I_2 inhibits the increase in A_2 concentration; Fig. S3B) and since each traveling wave of A_2 is followed by a traveling wave of I_2, the waves stop traveling where they meet (and hence do not cross each other; Fig. S3C). Thus, in the meeting point between traveling waves, a boundary with high A_2 concentration is formed.

This concentration of A_2 at the boundary is higher than in either of the traveling waves from which it is formed. This is because when two waves of A_2 approach each other, the cells between them start to receive, by diffusing from both waves, more A_2 than if there was only one traveling wave approaching. Since in equation (3), the A_2

auto-activation is non-linear (quadratic), this additional A_2 allows the A_2 to reach fast relatively high concentrations before the inhibitor waves arrive. This is why these boundaries may be sufficiently distinct and stable to define the seams between scutes in development.

Margins and initial conditions:

The margins are defined as two 13 cell-wide fringes spanning from the anterior to the posterior of the carapace. The initial conditions consist of two rows of A_1 concentration peaks (see Figs 1, 4) in these margins of the carapace. These peaks of A_1 have a constant concentration over the simulation time. The remaining cells in the margins do not produce A_1.

Growth:

Growth is implemented by adding cells in the midline. These additions occur at different rates along the anterior-posterior axis in a pattern derived from empirical observations. As a consequence, added cells displace a whole row of cells to the left and to the right from the midline.

From iteration 180000, growth rates double to represent an acceleration observed in carapace growth.

Bead experiments:

Beads are simulated by defining a position x,y (see Fig. S4 for the exact values) from which an additional amount of (a) A_1, A_2, I_1 or I_2 or (b) another factor B, upstream of one of these, diffuses with a rate of D_{BB}. In case (a), the additional amount of activator or inhibitor diffusing in each time step from the bead is added to the concentrations of A_1, A_2, I_1 or I_2, respectively, in the position [x,y] of the bead; in

case (b), B is added to or subtracted from the differential equation defining the change of concentration in the molecule affected by B. Since B represents an additional sort of molecule, it is given a diffusion rate D_B and degradation rate m_B. The time t_B when diffusion from the bead is initialized was set according to the respective *in vitro* experiment we wanted to simulate.

Natural and abnormal variation:

Configurations of scute numbers seen in species such as *Caretta caretta* or *Lepidochelys olivacea* can be found in the variational space of the model by increasing or decreasing the length of the anterior/posterior axis of the developing carapace.

In order to generate the scute anomalies reported in Figs 5, S7, and S8, we introduced two alternative changes in the model. In one (Fig. S7), the right half of the carapace gradually moves towards the anterior direction. The time at which this movement starts is t_{shift}. From then, the hemisphere is moved by one row every v_{shift} iterations and i_{shift} times, t_{shift}, v_{shift} and i_{shift} being model parameters. In the other (Fig. S8), lateral growth on the right side is, from the beginning, faster by a factor of add_R/add_L than growth in the left side. This means that the position-dependent rate at which cells were added along the midline is multiplied with add_R/add_L, respectively.

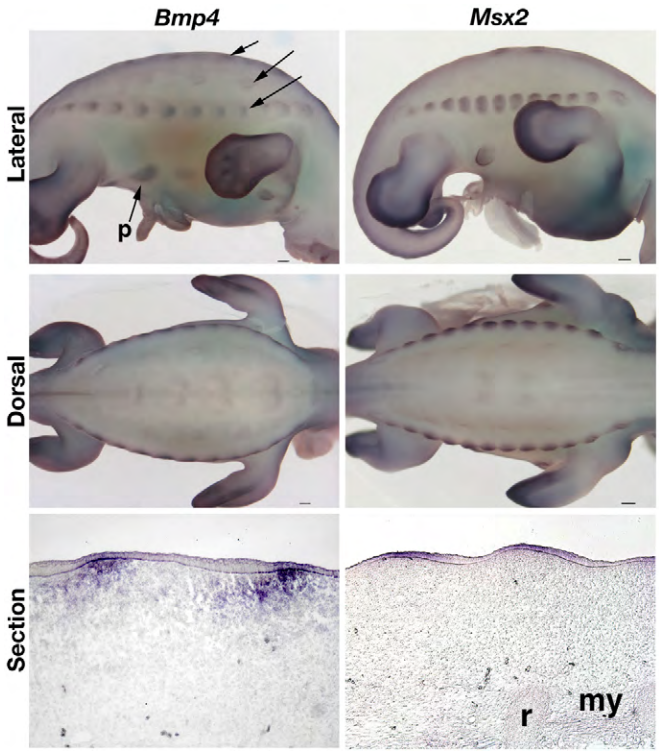

Fig. S1. Expression of *Bmp4* and *Msx2* viewed laterally, dorsally, and in section in stage Y16 *Trachemys* embryos. *Bmp4* and *Msx2* have overlapping expression patterns: the expression of *Bmp4* is stronger anteriorly in the developing scutes, whereas *Msx2* expression is seen along the protrusions of the carapacial ridge. Sections show that *Bmp4* is expressed in the mesenchyme and epithelium opposite the myotomes, and *Msx2* is expressed in the epithelium opposite the ribs. Arrows point to scute placodes. p, plastral scute placode; r, rib; my, myotome. Anterior is toward the right. Scale bars, 200 μm.

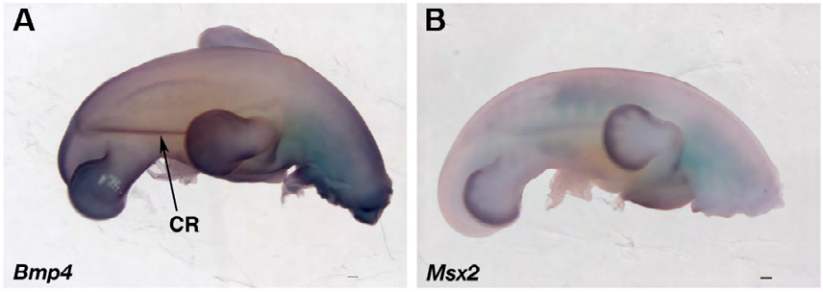

Fig. S2. Expression of *Bmp4* and *Msx2* in scuteless soft-shell *Pelodiscus* embryos. *Bmp4* and *Msx2* are expressed in a line along the carapacial ridge (CR). Anterior is toward the top. Scale bars, 200 μm.

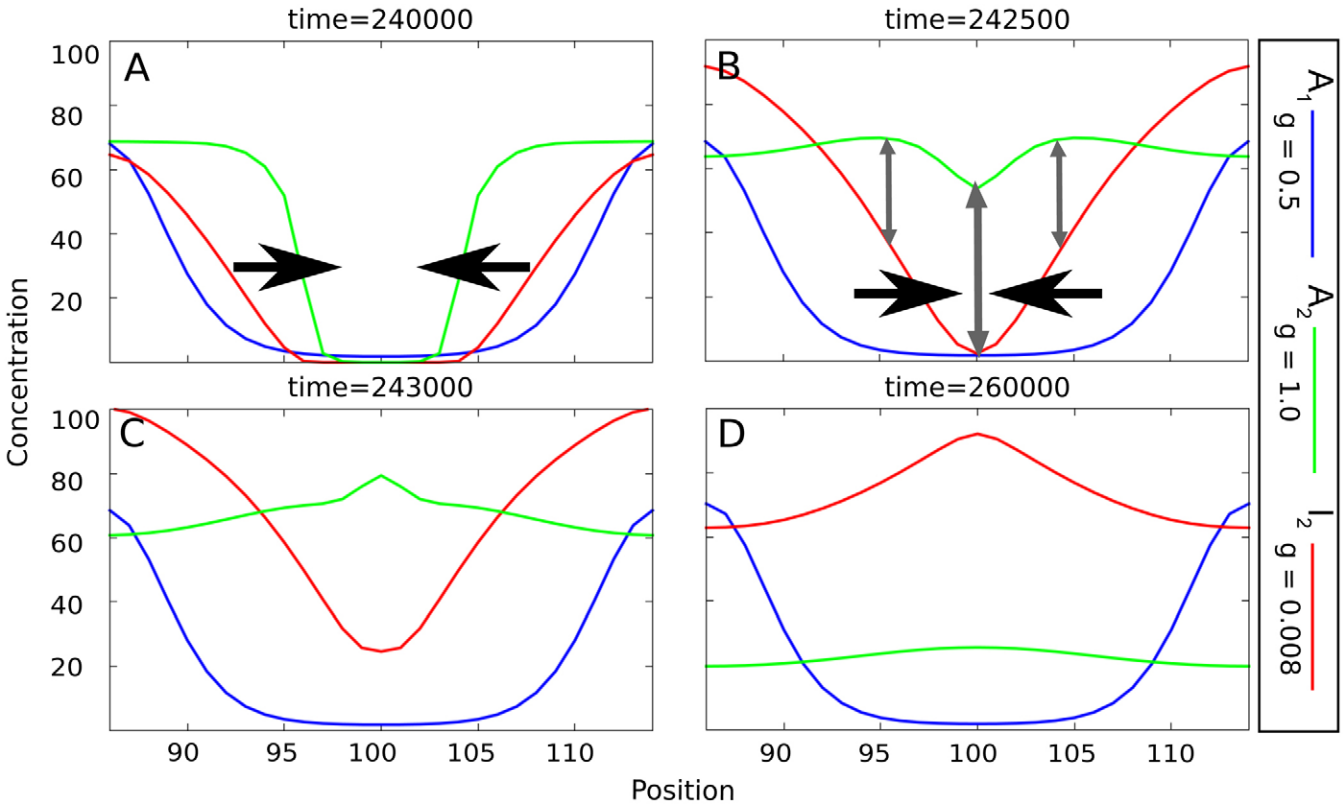

Fig. S3. 1-dimensional dynamics of colliding traveling waves. (A) From the spots of high A_1, activator A_2 is produced and diffuses away. Due to its activation by A_2, I_2 spreads with a delay. Vertical arrows stress the differences between A_2 and I_2 concentrations in different places; horizontal arrows indicate the direction of wave propagation. (B) While the waves approach due to diffusion, I_2 has already decreased A_2 concentration in those spots where it was produced first, preventing the A_2 wave from spreading backwards. This is why colliding waves stop (C). The contribution of both waves causes the difference between $[A_2]$ and $[I_2]$ to be highest at the collision point, leading to strong upregulation of A_2. This leads to a relatively stable gene expression peak in this place (D). A_1:blue lines; A_2:green lines; I_2:red lines. In all 1-dimensional graphs Y=20; 84<X<116. For clearer visualization, we set $m_3=m_4=0.1$, $r_2=0.25$, and rescaled the concentration of A_1 in the graph by the factor g=0.5, I_2 by the factor g=0.008.

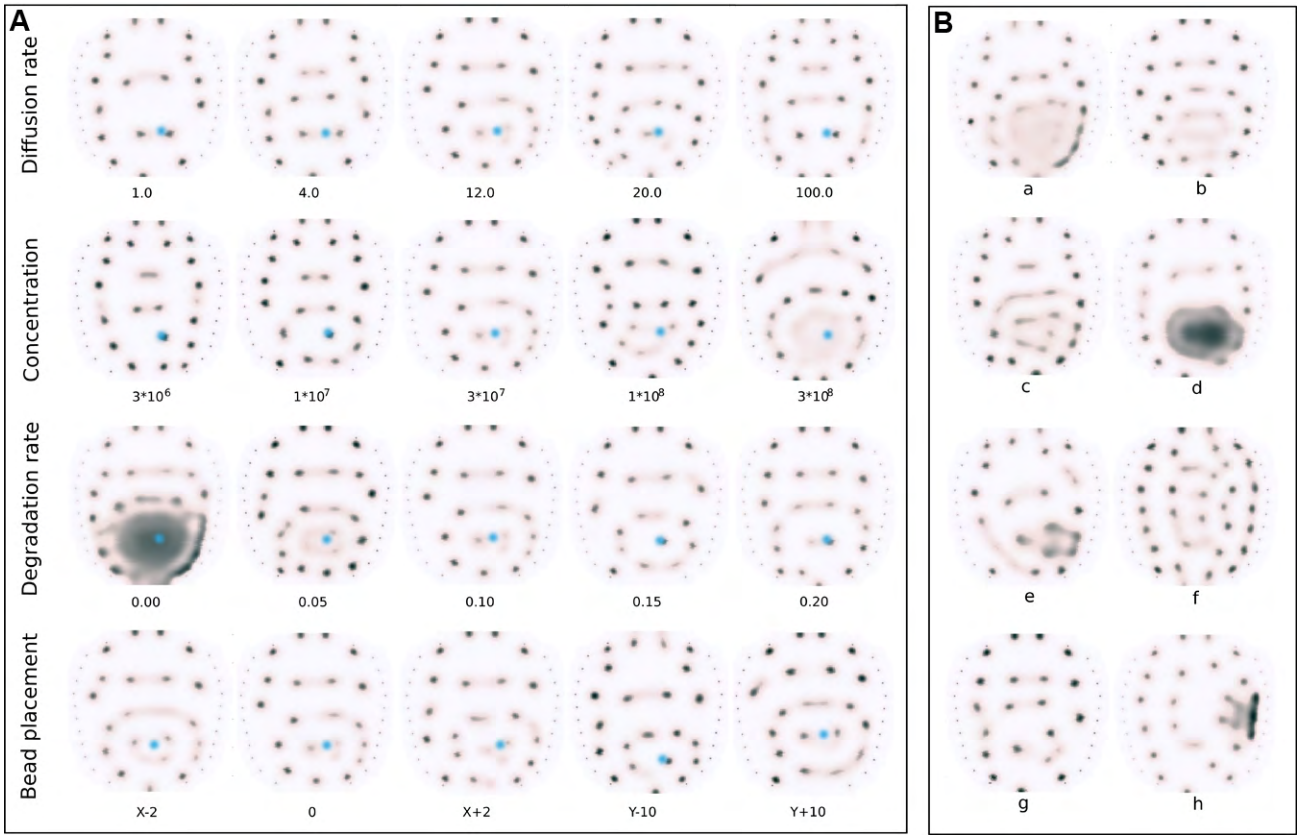

Fig. S4. Simulation of Inhibition of I_1 by bead implantations in a 5-dimensional parameter space. (A) For the basic model parameters given in the methods, a diffusible Factor B was allowed to diffuse from a certain position (X,Y) with a diffusion rate D and a degradation rate μ. The initial concentration in the bead is defined by B(0). For the comparison with a SHH-bead experiment shown in Figure 4, the following parameters were chosen: D=12.0, μ=0.1, B(0)=$3*10^7$, X=40, Y=105. Here, in every row, one parameter has been changed in the way indicated. The plots show the concentration of A_1 at t=210000. Units are AU. Bead positions are marked blue. (B) An overview of patterns produced by different combinations of the parameters listed above. a) D=15.0, μ=0.01, B(0)=$2*10^7$, X=45, Y=111. b) D=15.0, μ=0.05, B(0)=$3*10^7$, X=40, Y=103. c) D=15.0, μ=0.01, B(0)=$1*10^7$, X=43, Y=109. d) D=5.0, μ=0.01, B(0)=$3*10^7$, X=40, Y=107. e) D=5.0, μ=0.01, B(0)=$1*10^7$, X=45, Y=113. f) D=100.0, μ=0.0, B(0)=$1*10^7$, X=65, Y=110. g) D=5.0, μ=0.1, B(0)=$3*10^7$, X=45, Y=105. h) D=4.0, μ=0.0, B(0)=$1*10^7$, X=65, Y=110.

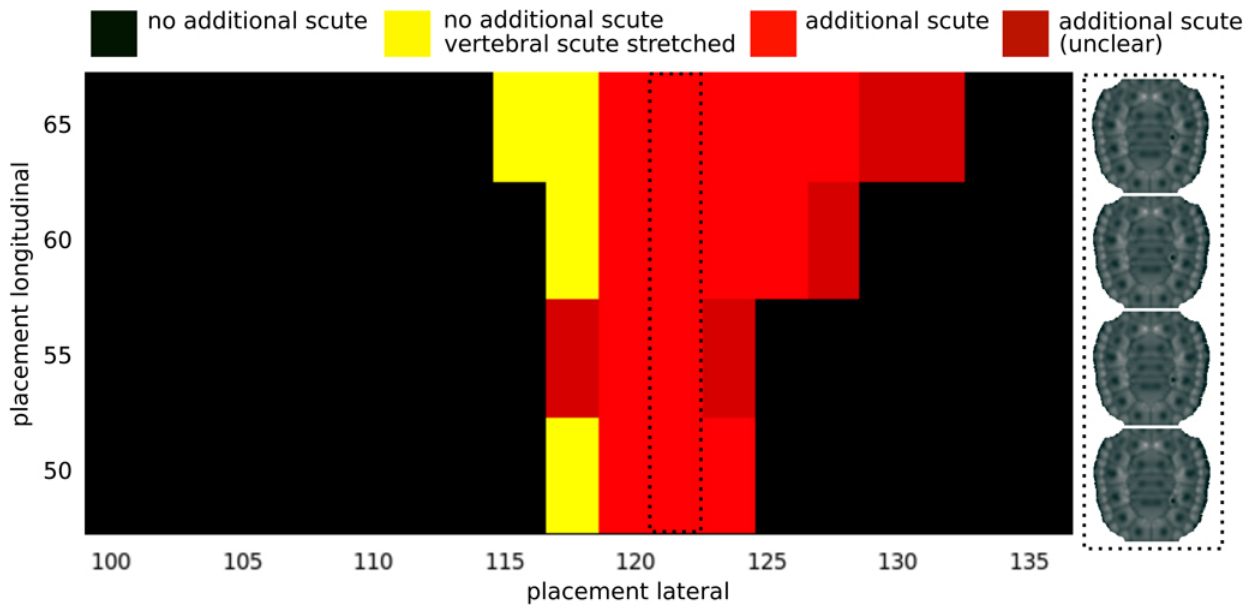

Fig. S5. **Simulation of Activation of A_2 by bead implantations.** For the basic model parameters, A_2 was allowed to diffuse from a bead position X,Y and an initial concentration $A_2(0)=10^5$. The figure shows the morphospace for different positions of the bead. It can be shown that the total variation obtained is relatively low, since only three distinct types of morphologies emerge: lengthening of vertebral scutes, one additional scute, and the normal phenotype. The parameter range in which additional scutes emerge is limited so that it highly depends on the placement of the bead whether or not any phenotypic change is obtained at all. The plots show the concentration of A_2 at t=240000; their position in the parameter space plot is delineated by spotted lines. A lateral position of x=100 localizes the midline.

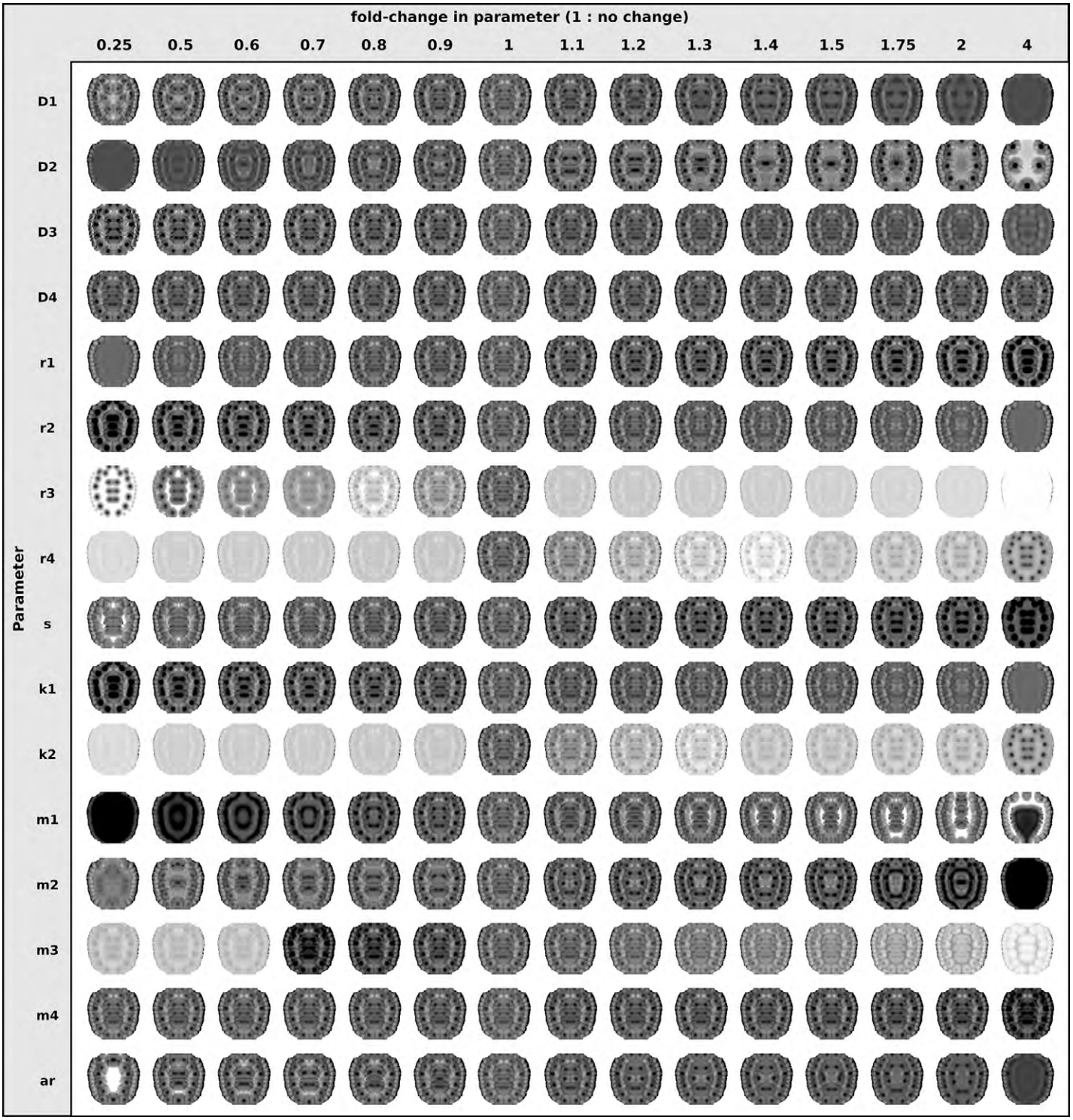

Fig. S6. Variation by parameter choices. All relevant parameters, as explained in supplementary materials and methods text, were individually modified by multiplying the original values by factors between 0.25 – 4.0, as noted on the horizontal axis. The plots show concentration of A_2 at time=240000, if run with the respective parameter value.

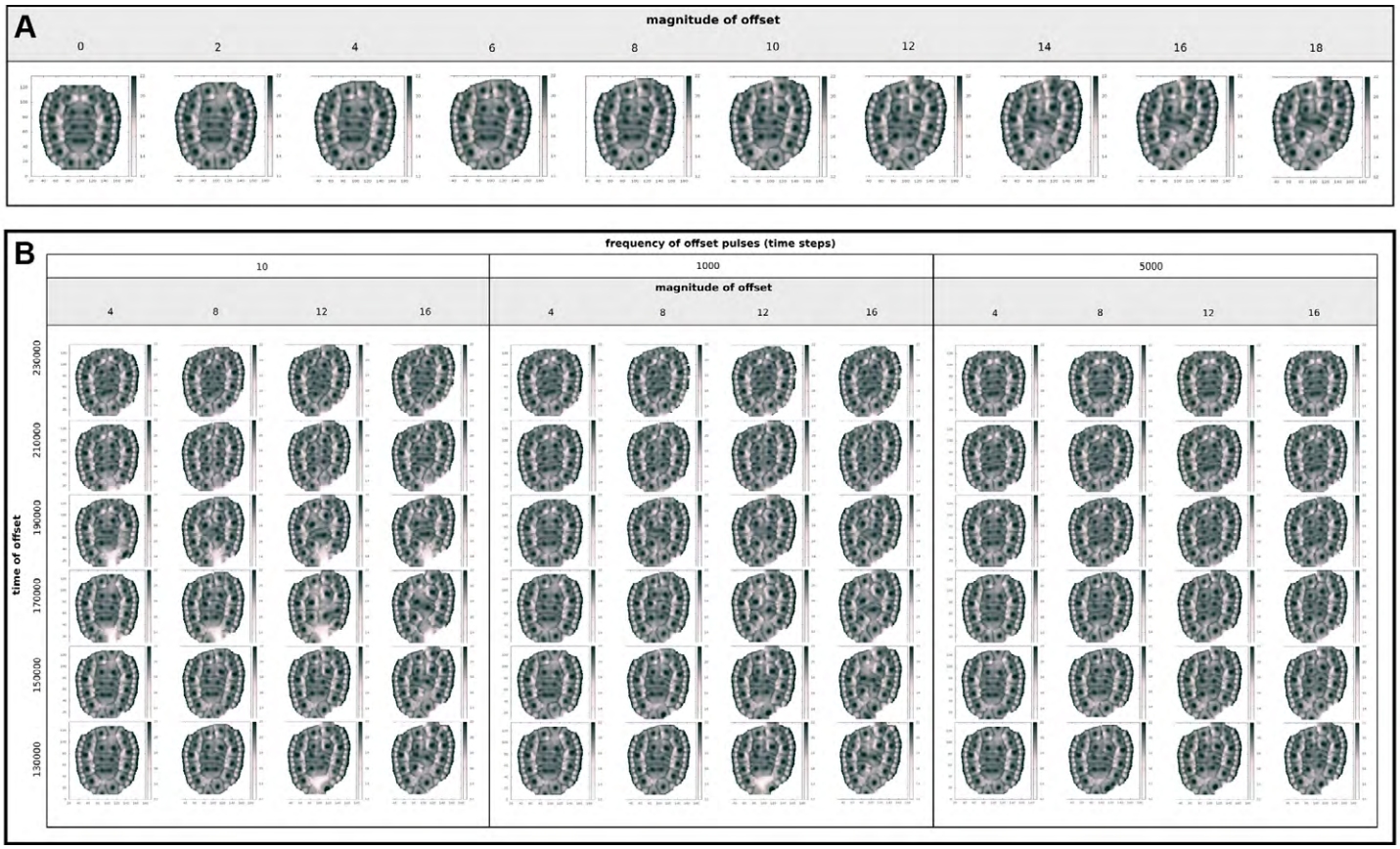

Fig. S7. Variational space of resulting scute patterns from the introduction of lateral offsets to the prepattern in the model. (A) A slight offset of various magnitudes (total number of cell rows shifted) to the right side in the anterior direction was immediately introduced into the pre-pattern. (B) Both the time (y-axis) and the frequency of offset pulses (every 10, 1000 and 5000 time steps; 3 panels) were varied in addition to the magnitude of offset (4 columns per panel). Time is given in simulation steps. The magnitude of offset is quantified in terms of grid cells shifted. In all pictures, the final expression of A2 is shown.

Fig. S8. Variational space of resulting scute patterns from the introduction of differential growth in the model. The introduction of differential growth to the model such that one side grows at different rates than the opposite side produces supernumerary scutes asymmetrically in varying patterns. The rates of growth acceleration in the left or right hemisphere are given by the figure axes.

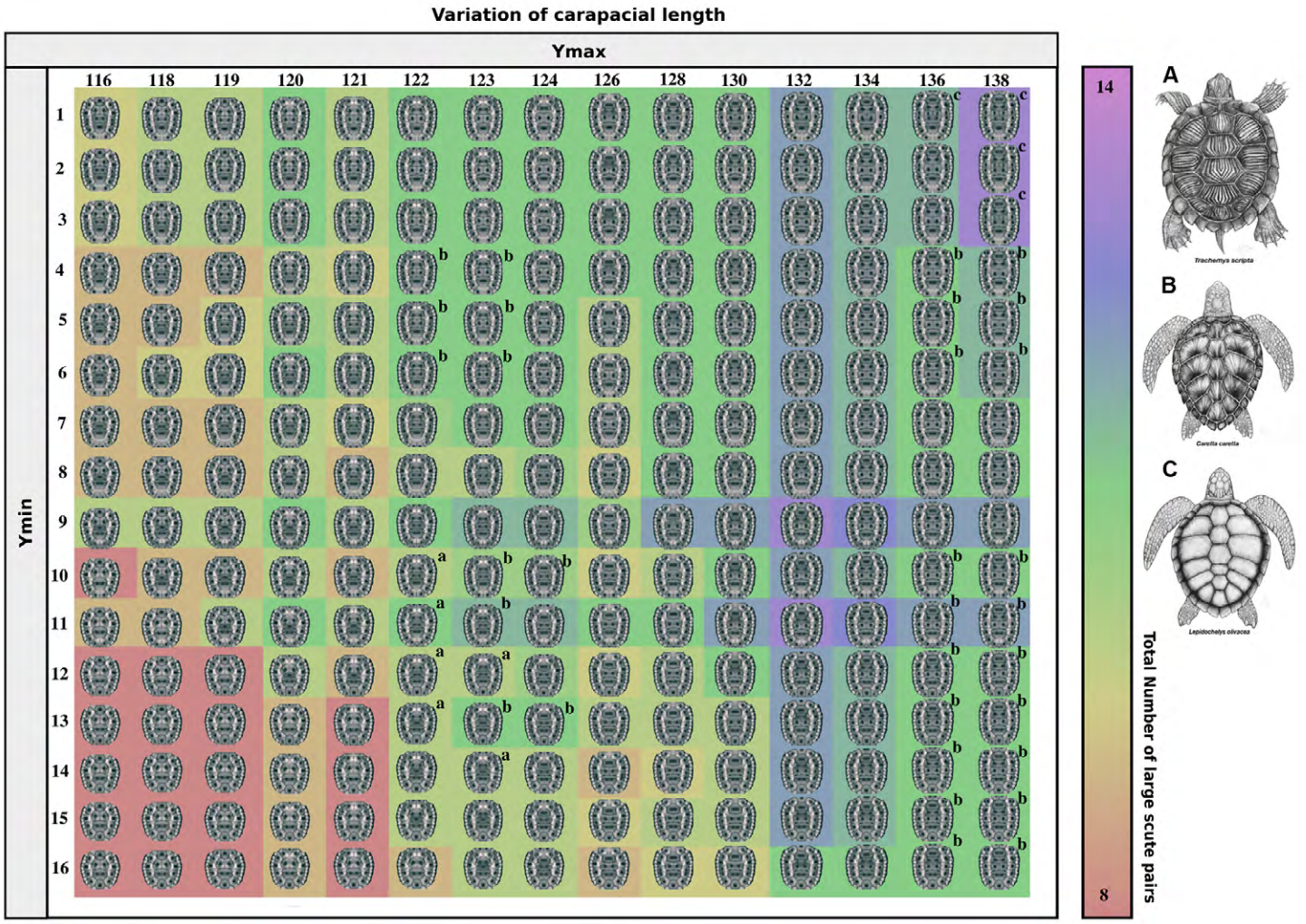

Fig. S9. **Natural interspecific variation in scute numbers reproduced by the model.** Most turtles have 4 costal and 5 vertebral scutes, as seen in *Trachemys scripta* (A). Some sea turtles, such as *Caretta caretta* (B) and *Lepidochelys olivacea* (C) have 5 or 6-7 costal scutes, respectively. *L. olivacea* also has an additional vertebral scute. By shortening or lengthening the anterior/posterior axis prior to the induction of the marginal scute placodes, additional costal and vertebral scutes are produced. Here, the axes of the figure assign the position of the anterior (Ymax) and posterior (Ymin) boundaries of the carapace. Colors illustrate the total number of vertebral scutes and costal scute pairs. Scute configurations that correspond to the numbers observed in these species have been marked with corresponding letters a, b, c and outlined. Independently of the subjectivity of the process of counting, the scute number is not correlated with an elongation of the anterior/posterior axis in a simply linear manner. Therefore, there are several possible trajectories to evolve from the configuration of *T. scripta* to the configuration of *C. caretta* within the morphospace.

Movie 1. Micro-computed tomography. Stage Y16 *Trachemys* fixed in 4% PFA and dyed with phosphotungistic acid in 70% ethanol for 24 hours (Metscher, 2009). The sample was imaged with a custom-built µCT system Nanotom 180 NF to obtain scans with an effective voxel size of 5 µm. The reconstruction was then down-sampled to 10 µm voxel resolution and Avizo Fire 6.3 was used to render the 3D movies. iMovie 11 (Apple) was used to join the frontal (left) and lateral (right) movies. In the lateral movie, anterior is right.

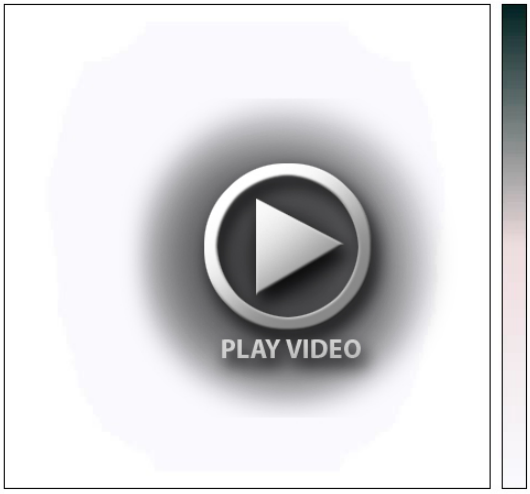

Movie 2A.

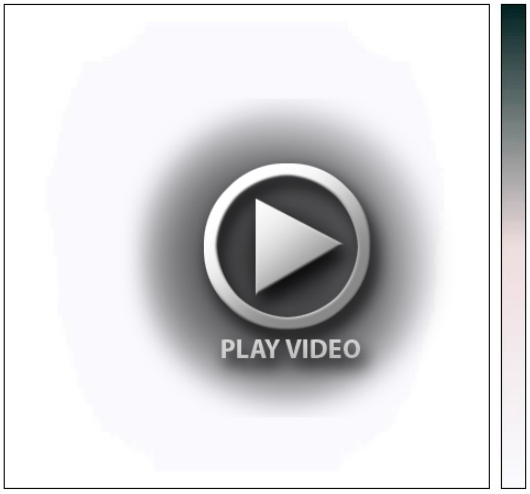

Movie 2B.

Movie 2. Movie of the mathematical models of turtle scute formation. (A) From a pre-pattern of 12 marginal spots at t=0, a first activator-inhibitor couplet coupled with growth (shown left) sets the relative positions of the presumptive scute placodes, resulting in two columns of 12 marginal, 4 costal, and 6 vertebral scute primordia (t=230000). A second reaction-diffusion system (shown right), activated by the first reaction-diffusion system, generates the final scute architecture by traveling waves, resulting in 24 marginal, 8 costal, and 6 vertebral (5 vertebral plus 1 nuchal) scutes, as seen in *Trachemys*. (B) High time resolution version of the second reaction-diffusion system to better illustrate its properties. FFmpeg (http://ffmpeg.org/) was used to create these movies.